Magnetotail total pressure and lobe magnetic field at onsets of sawtooth events and their relation to the solar wind

Chao-Song Huang[1] and Xia Cai[2]

Received 7 October 2008; revised 30 December 2008; accepted 10 February 2009; published 10 April 2009.

[1] Sawtooth events in the Earth's magnetosphere are global, large-amplitude oscillations of energetic plasma particle fluxes at geosynchronous orbit and represent periodic magnetospheric substorms with a typical period of ~3 hours. Sawtooth events generally occur during magnetic storms, when the magnetosphere is continuously driven by southward interplanetary magnetic field and high-speed solar wind stream. However, it has not been well understood how the magnetotail parameters (the total pressure, the lobe magnetic field, and the tail lobe total magnetic flux) at the onset of sawtooth events are related to the solar wind driver. In this study, we conduct a statistical analysis of the magnetotail parameters measured by the Geotail satellite during sawtooth events over 1998–2006. At the onset of sawtooth events (storm-time substorms), the magnetotail total pressure and the lobe magnetic field increase with the solar wind pressure and merging electric field, and the total magnetic flux in the tail lobe increases with the merging electric field. Empirical formulas of the relationship of the magnetotail parameters at the sawtooth onset and the solar wind are derived for the first time. We have made a superposed epoch analysis. The magnetotail total pressure and lobe magnetic field take 52 min for gradual buildup and then 26 min for rapid increase before the sawtooth onset, and they decrease for 77 min after the onset. We have also compared our results with previous studies on quiet time tail behavior and isolated substorms. The magnetotail total pressure at the sawtooth onset is about three times that of the quiet time magnetotail, and the lobe magnetic field at the sawtooth onset is 8–10 nT higher than the quiet time value. The results imply that the sawtooth onset occurs when the magnetotail reaches a critical state and that the critical state depends on the solar wind parameters. Our findings provide new insights into the storm-time magnetospheric dynamics and important guidance for model simulations.

Citation: Huang, C.-S., and X. Cai (2009), Magnetotail total pressure and lobe magnetic field at onsets of sawtooth events and their relation to the solar wind, *J. Geophys. Res.*, *114*, A04204, doi:10.1029/2008JA013807.

1. Introduction

[2] Sawtooth events in the Earth's magnetosphere are global, large-amplitude oscillations of energetic plasma particle fluxes at geosynchronous orbit. The plasma particle fluxes show a well-defined ''sawtooth'' shape, with gradual decreases followed by rapid increases. Very similar variations of electron and proton fluxes are detected nearly simultaneously over a large local time range on the nightside. In early studies [*Borovsky et al.*, 1993; *Belian et al.*, 1995], the recurrent injections of the plasma particle fluxes at geosynchronous orbit were termed periodic substorms. *Huang* [2002] and *Huang et al.* [2003b] have found that each plasma particle flux injection is related to a magnetic reconnection onset in the midtail and plasmoid formation. *Huang et al.* [2003a, 2003b, 2004, 2005], *Reeves et al.* [2003], *Lee et al.* [2004], *Lui et al.* [2004], *Clauer et al.* [2006], *Henderson* [2004], and *Henderson et al.* [2006a, 2006b] have analyzed multiple space-based and ground-based instrumental measurements of sawtooth events. These studies show that each cycle of sawtooth oscillations includes an injection of energetic plasma particles from the tail to the inner magnetosphere, a magnetic dipolarization of the magnetotail, and all other signatures of substorms. The region of dispersionless flux injections during sawtooth events can extend to the dayside [*Huang et al.*, 2003a, 2003b, 2005; *Henderson et al.*, 2006a, 2006b], in contrast to the flux injections of quiet time substorms that are mostly limited to the midnight sector. Sawtooth oscillations often occur periodically with a typical period of ~3 hours. Some investigators suggested that sawtooth events are driven by extremely strong solar wind and that periodic substorms are driven by relatively weak (but still strong) and continuously southward interplanetary magnetic field (IMF). However, sawtooth events have all well-known characteristics of magnetospheric substorms, and it is becoming widely accepted that sawtooth events are periodic substorms.

[1]Institute for Scientific Research, Boston College, Chestnut Hill, Massachusetts, USA.
[2]Bradley Department of Electrical and Computer Engineering, Virginia Tech, Blacksburg, Virginia, USA.

0148-0227/09/2008JA013807

[3] A sawtooth event is a series of individual tooth events, and each individual tooth represents one substorm. The substorm activity during sawtooth events can last many cycles under continuous southward IMF conditions. The first cycle is often related to a solar wind pressure impulse, but the subsequent cycles often occur without obvious change in the solar wind. In other words, the substorm onset during sawtooth events does not require external trigger. Similarly, isolated substorms can also occur without external triggers [*Henderson et al.*, 1996], although many isolated substorms are indeed correlated with IMF northward turning and/or solar wind pressure enhancement [*McPherron et al.*, 1986; *Lyons et al.*, 1997; *Hsu and McPherron*, 2003].

[4] *Huang et al.* [2003a, 2004] suggested the following scenario to explain the generation of periodic substorms. Magnetospheric substorm processes have an intrinsic cycle time of ~3 hours. The magnetosphere takes ~3 hours after one substorm onset to reach the state for the next onset to occur. Each cycle of the periodic substorms can occur under stable IMF and solar wind conditions, and the onset does not have to be triggered by either a northward IMF turning or a solar wind pressure impulse. A sudden change in the solar wind can trigger a substorm onset if and only if the magnetosphere has reached the critical state conducive to the generation of substorms. In the case of no external triggering from the solar wind, substorms will still occur when the magnetosphere has reached the unstable state, and an internal plasma instability can trigger substorm onsets.

[5] Substorms can be divided into two categories according to the geomagnetic activity: the quiet time isolated substorms and storm-time substorms. The magnetospheric-ionospheric disturbances (such as the plasma particle flux injections at geosynchronous orbit, magnetotail magnetic dipolarization, *AL* index, and auroral intensity) associated with storm-time substorms are generally much stronger than those of isolated substorms. It was speculated whether the magnetospheric dynamics of storm-time substorms are different from quiet time substorms. *Baumjohann et al.* [1996] found that the magnetic field dipolarization and the earthward convection in the near-Earth tail are much more pronounced for storm-time substorms than for nonstorm substorms. *McPherron and Hsu* [2002] compared the two types of substorms and concluded that the differences between the various classes are the absolute value of the lobe field and the size of the changes. When the data are normalized to unit field amplitude, the percent change during storm-time and non–storm-time substorms is nearly the same. *Henderson et al.* [2006a, 2006b] showed that most of the sawtooth injections are predominantly caused by unusually large and longitudinally extended substorms. During sawtooth events, each tooth is associated with a wider-than-usual, dispersionless injection region, and a localized auroral onset develops on the lower branch of a thinned double-oval distribution. *Cai et al.* [2006] analyzed ionospheric potential patterns and found that in terms of ionospheric electrodynamics, the sawtooth events have features similar to those of isolated substorms, though larger in spatial extent and in magnitude. *Pulkkinen et al.* [2006, 2007] modeled the magnetospheric current system during storm-time sawtooth events. They found that the tail field behavior resembles that of nonstorm substorms and concluded that the sawtooth events do not represent a specific class of magnetospheric activity. *DeJong et al.* [2007] found that the polar cap open magnetic flux during sawtooth events is, on average, 1.5 times the flux during isolated substorms and steady magnetospheric convection (SMC) events.

[6] An outstanding problem in the study of substorms is whether the magnetotail reaches a critical point prior to the onset of a substorm. Substorms are often described as an energy loading-unloading process [*Russell and McPherron*, 1973; *Baker et al.*, 1996]. The solar wind energy is stored in the magnetotail during the growth phase of substorms, the substorm onset occurs when the magnetosphere reaches a critical state, and the energy in the magnetotail is released during the expansion phase. *Nakai and Kamide* [2003, 2004] found that the magnetic field in the magnetotail just prior to the substorm expansion onset correlates well with the Dst index and that the magnetotail total pressure values at the substorm onset are distributed near the upper limit of all data (including nonsubstorm data and substorm events). *Shukhtina et al.* [2004] derived the quantitative relationship among the magnetotail parameters (the lobe magnetic field, flaring angle, and tail radius) and solar wind parameters for different magnetospheric states, including the substorm onsets, steady magnetospheric convection, and quiet periods. *Shukhtina et al.* [2005] showed that the total magnetic flux in the magnetotail at the substorm onset is linearly correlated with the merging electric field integrated over 60 min prior to the onset. These studies concentrate on quiet time isolated substorms.

[7] Sawtooth events generally occur during magnetic storms when the magnetosphere is continuously driven by southward IMF. The magnitudes of the southward IMF and solar wind velocity during storm times are much larger than those at quiet times. Although previous studies have shown that the characteristics of storm-time sawtooth events are qualitatively similar to those of quiet time substorms, it is still unknown whether the magnetospheric state at the onset of sawtooth events is the same as that for quiet time substorms. In this study, we conduct a statistical analysis of sawtooth events measured by the Geotail satellite and use a method similar to that described by *Nakai and Kamide* [2003, 2004] to find the critical magnetospheric state. Our purpose is to find what the magnetospheric parameters (the magnetotail total pressure, the lobe magnetic field, and the total magnetic flux in the tail lobe) at the onset of sawtooth events are, how these critical magnetospheric parameters are related to the solar wind driver and to possible internal driving mechanism, and whether the critical magnetospheric condition for the onset of sawtooth events is different from that for isolated substorms.

2. Observations

2.1. An Example of Sawtooth Events

[8] We first present an example of sawtooth events. This case occurred during the magnetic storm on 17–20 April 2002. Figure 1a shows the solar wind dynamic pressure and the IMF B_z component measured by the Advanced Composite Explorer (ACE) satellite located at ~220 R_E during 18 April 2002. The solar wind data have been shifted to the Earth's bow shock nose with the minimum variance analysis technique developed by *Weimer et al.* [2003]. In all cases analyzed in this paper, the solar wind and IMF data have been

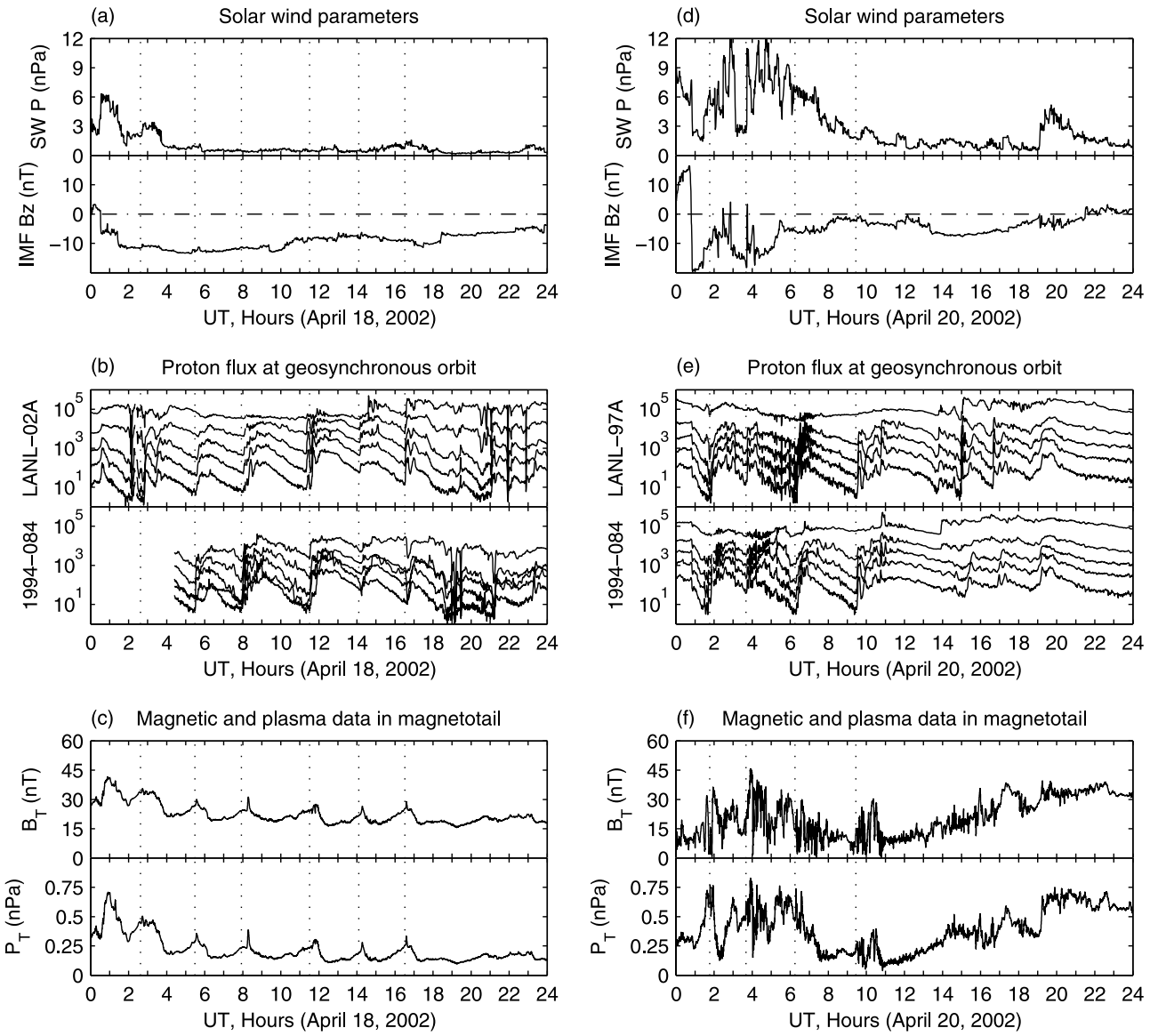

Figure 1. An example of sawtooth events. (a) Solar wind dynamic pressure and interplanetary magnetic field (IMF) B_z measured by the ACE satellite, (b) proton flux measured by geosynchronous satellites, and (c) magnetotail magnetic field and total pressure measured by the Geotail satellite on 18 April 2002. (d–f) Same as Figures 1a–1c but for 20 April 2002. The dotted vertical lines denote substorm onsets.

shifted to the bow shock nose with the above technique and are presented in the GSM coordinate. As can be seen in Figure 1a, the solar wind pressure showed an enhancement around 0100 UT and then became small after 0500 UT, and the IMF B_z was continuously negative and stable for the entire day.

[9] Figure 1b displays the proton flux measured by the LANL-02A and 1994-084 geosynchronous satellites. The energy channels of the proton flux are 50–75, 75–113, 113–170, 170–250, and 250–400 keV. The variations of the proton flux show a well-defined sawtooth-like shape, with a gradual decrease followed by a sudden increase. The sawtooth events on 18 April 2002 have been analyzed in detail by *Huang* [2002], *Huang et al.* [2003b, 2005], and *Henderson et al.* [2006a]. The gradual decrease of the proton flux occurs when the magnetotail becomes more stretched during the growth phase of substorms, and the sudden increase of the flux corresponds to the flux injection from the tail to the inner magnetosphere at the expansion onset. The sawtooth-like variations of the flux represent a series of substorms with a period of ~3 hours. In this paper, we use the same criteria to identify sawtooth events as those of *Cai et al.* [2006] and *Cai and Clauer* (Investigation of the period of sawtooth events, manuscript submitted to *Journal of Geophysical Research*, 2009): At least one geosynchronous satellite is located around local noon (3 MLT hours from local noon) and one around local midnight (3 MLT hours from local midnight), and the plasma particle flux injection is observed globally. The vertical dotted lines in Figure 1b denote the times of the flux injections (substorm onsets).

[10] Shown in Figure 1c are the magnetotail magnetic field and total pressure measured by the Geotail satellite. In this

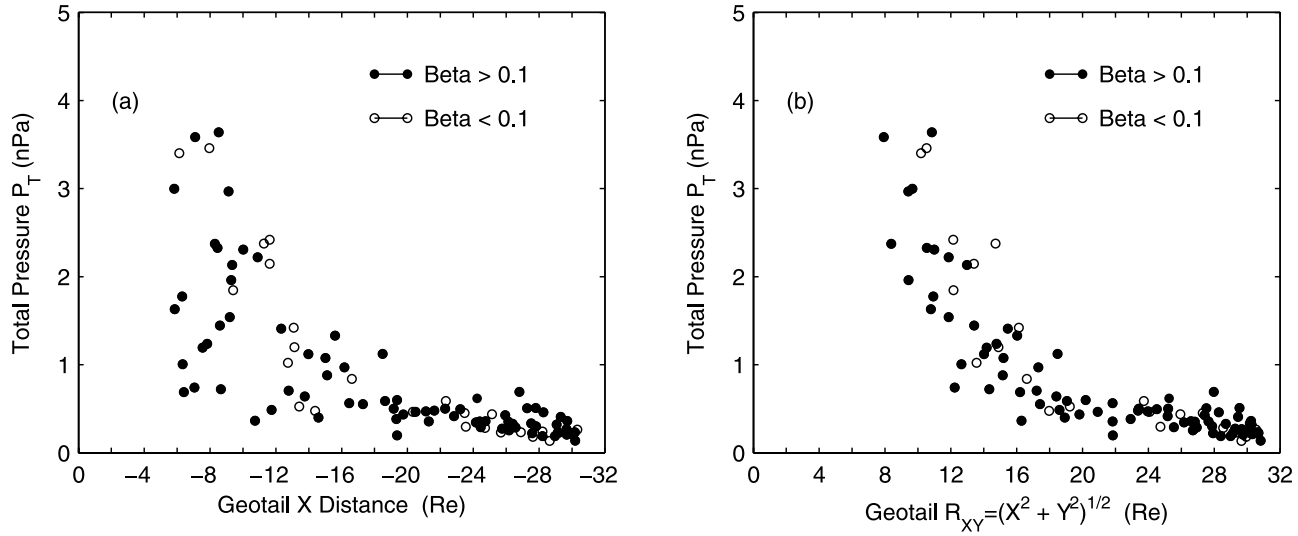

Figure 2. The magnetotail total pressure at the onset of storm-time substorms during sawtooth events as a function of (a) the X distance and (b) the radial distance R. The dots and open circles represent the data with the ion β values of larger than 0.1 and smaller than 0.1, respectively.

study, all magnetotail data were measured by the Geotail satellite. The magnetic field data have a time resolution of 3 s [*Kokubun et al.*, 1994], and the plasma particle data have a time resolution of 12 s [*Mukai et al.*, 1994]. During the entire day of 18 April 2002, the Geotail satellite was located in the midtail, and the GSM coordinate of Geotail was between (−22.19, 13.83, 12.49) and (−29.32, 4.56, 8.55) R_E. Because of the position in the Z axis, Geotail was in the northern lobe. In Figure 1c, the magnetic field strength and magnetotail total pressure are given by $B_T = (B_x^2 + B_y^2 + B_z^2)^{1/2}$ and $P_T = B_T^2/2\mu_0 + N_i k(T_i + T_e)$, where N_i is the ion density and T_i is the ion temperature. We take $T_e = T_i/7$ in the calculations of the total pressure [*Baumjohann*, 1993; *Shukhtina et al.*, 2004].

[11] The magnetic field shows a very regular periodic variation with a period of ∼3 hours, which is caused by the periodic generation of plasmoids in the midtail. The detailed characteristics of the plasmoids in this case have been analyzed by *Huang* [2002]. According to the near-Earth neutral line model of magnetospheric substorms [*McPherron et al.*, 1973; *Hones*, 1984; *Baker et al.*, 1996; *Nagai et al.*, 1998], magnetic reconnection occurs in the tail between −20 and −30 R_E on the closed field lines of the central plasma sheet at the onset of a substorm. The reconnection creates a structure of closed magnetic loop which is termed the plasmoid. After the lobe reconnection begins, the plasmoid is released and travels tailward at high speeds (500–1000 km s^{-1}). In Figure 1c, the magnetic field strength increases before each substorm onset, the spike in the magnetic field strength after the onset represents the lobe magnetic field compressed by the plasmoid moving tailward through the satellite [*Slavin et al.*, 1984; *Taguchi et al.*, 1998], and then the field strength decreases. The magnetotail total pressure shows similar periodic variations. Because Geotail was in the lobe, the total pressure in the magnetotail in this case is essentially the magnetic pressure.

[12] The Geotail satellite was continuously in the magnetotail during the long-lasting magnetic storm of 17–20 April and moved into the plasma sheet on 20 April. Geotail was located between (−25.10, −6.43, 1.32) and (−17.30, −11.09, 1.13) R_E during 0000 and 1200 UT on 20 April. Plotted in the right column of Figure 1 are the solar wind pressure and IMF B_z (Figure 1d), the proton flux at geosynchronous orbit (Figure 1e), and the magnetic field strength and magnetotail total pressure in the plasma sheet measured by Geotail (Figure 1f) on 20 April. The vertical dotted lines denote the flux injections (substorm onsets). In this case, Geotail provided the measurements of the plasma sheet parameters during the sawtooth event.

2.2. Magnetotail Parameters at the Onsets of Sawtooth Events

[13] The purpose of this paper is to conduct a statistical analysis of the magnetotail parameters at the substorm onset and their relation with the solar wind during sawtooth events. We searched the plasma particle flux data measured by the LANL geosynchronous satellites over 9 years (1998–2006) and found 107 sawtooth events during which there are 431 individual teeth in total. We then searched the Geotail satellite data and found 33 sawtooth events with 101 individual teeth during which Geotail was in the magnetotail with $X < -8$ R_E. These 101 teeth (substorms) occurred during magnetic storms, and the mean value of the Dst index at the substorm onsets is −68 nT. All statistical analysis given below is based on the 101 substorms. Considering that the magnetotail parameters vary with time, we averaged the Geotail data over 5 min prior to each onset of the substorms and use the averaged value to represent the parameters at the onset in the following statistics. In order to distinguish the difference between the sawtooth events and quiet time substorms, we use the term, "sawtooth onset", to represent the onset of the individual tooth (substorm) during sawtooth events.

[14] Figure 2 shows the magnetotail total pressure at the sawtooth onset as a function of the X distance and the radial distance R, respectively. Note that $R = (X^2 + Y^2)^{1/2}$ is the distance in the $X - Y$ plane. This is not significantly different from $(X^2 + Y^2 + Z^2)^{1/2}$ because the orbit of Geotail is close to

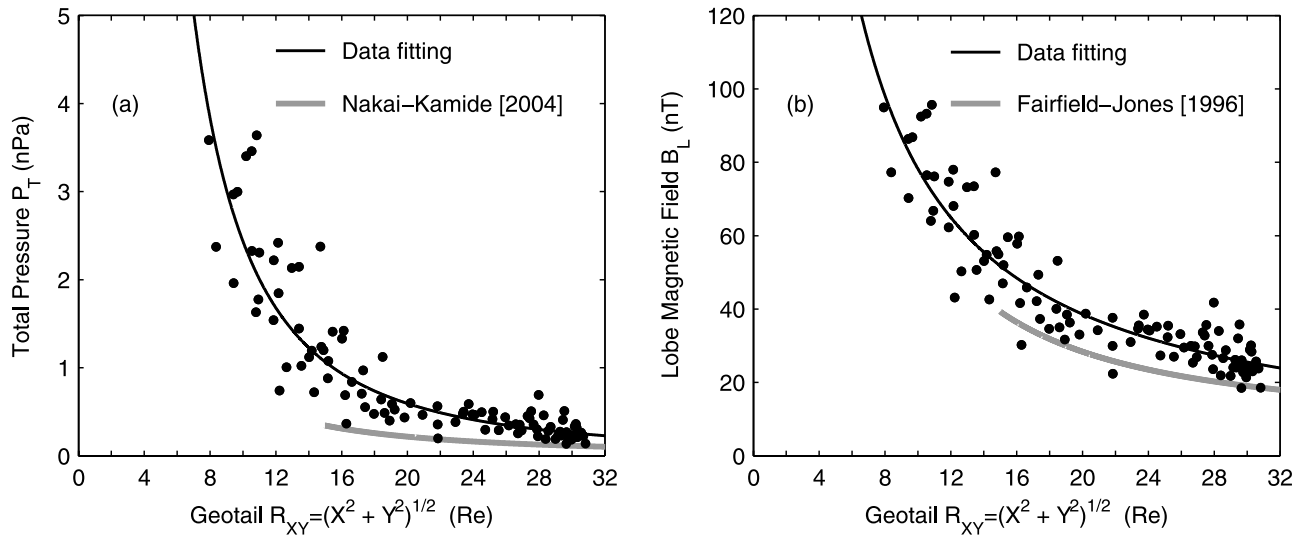

Figure 3. (a) The magnetotail total pressure and (b) the equivalent lobe magnetic field at the sawtooth onset as a function of the R distance. The black solid line is the regression line derived from the data of this study. The gray line is the result of previous investigations and plotted for comparison.

the equatorial plane. The magnetotail total pressure decreases with both the X distance and radial distance R, but the data are much better organized with R. The ion β, which is the ratio of the ion pressure to the magnetic pressure, $\beta = N_i kT_i/(B^2/2\mu_0)$, is often used to distinguish the different regions in the magnetotail. We assume that Geotail is in the plasma sheet for $\beta > 0.1$ and in the tail lobe for $\beta \leq 0.1$ [e.g., *Baumjohann et al.*, 1990; *Mukai et al.*, 1996; *Slavin et al.*, 2003]. There are 78 teeth when Geotail was in the plasma sheet ($\beta > 0.1$) and 23 teeth when Geotail was in the tail lobe ($\beta \leq 0.1$). The plasma sheet and tail lobe events are displayed by dots and open circles, respectively, in Figure 2. The plasma sheet events and lobe events do not show any noticeable difference in the distribution along R, which is because the plasma sheet pressure is balanced by the lobe pressure in the vertical direction. In the following, we will no longer separately consider the plasma sheet and lobe events, and the analysis will include all events.

[15] Figure 3a shows how the magnetotail total pressure at the sawtooth onset varies with the radial distance R. The black line is the data regression line derived with least squares fitting from our data set. The empirical formula of the magnetotail total pressure is given by

$$P_T = 264R^{-2.035} \tag{1}$$

where P_T is measured with nPa, and R is measured with R_E. All empirical formulas derived in this paper are valid for $8\ R_E < R < 31\ R_E$ because the data were measured by Geotail in this range. The gray line in Figure 3a is the distribution of the magnetotail total pressure derived by *Nakai and Kamide* [2004] mostly for cases without substorms and may be used as the quiet time reference. *Nakai and Kamide* [2004] identified 37 isolated substorm events and found that the total pressure at the onset is near the upper limit of all data points. It is seen from Figure 3a that the magnetotail total pressure at the sawtooth onset is always higher than the quiet time pressure. If we use the regression lines for a comparison, the difference between the magnetotail total pressure at the sawtooth onset and the quiet time value varies from 0.72 nPa at 15 R_E to 0.15 nPa at 30 R_E, and the ratio of the total pressure at the sawtooth onset to the quiet time value varies from 3.2 at 15 R_E to 2.3 at 30 R_E.

[16] The equivalent lobe magnetic field at the sawtooth onset is plotted in Figure 3b. The equivalent lobe magnetic field is defined as $B_L^2/2\mu_0 = B_T^2/2\mu_0 + N_i k(T_i + T_e)$ and includes the contribution of the plasma pressure. We will term it the lobe magnetic field for simplicity in the following. The data regression line can be expressed as

$$B_L = 814R^{-1.0175} \tag{2}$$

where B_L is measured with nT. The gray line is derived by *Fairfield and Jones* [1996] from 11 different space craft over a 20-year period. The lobe magnetic field at the sawtooth onset in our cases is 8–10 nT higher than that by *Fairfield and Jones* [1996] in the range of R = 15–30 R_E.

2.3. Relationship of Critical Magnetotail Parameters to Solar Wind Driver

[17] We now study how the magnetotail total pressure and lobe magnetic field in the midtail vary with the solar wind. As identified by *Nagai et al.* [1998], the magnetic reconnection site for substorms is between -20 and -30 R_E. For storm-time sawtooth events, the magnetic reconnection may occur in a location closer to the Earth. *Huang* [2002] analyzed the detailed characteristics of the plasmoids during the sawtooth event on 18 April 2002 and found that the magnetic reconnection might occur around $X_{\mathrm{GSM}} \sim -20\ R_E$. This inferred reconnection site is near the earthward end of the reconnection region derived by *Nagai et al.* [1998]. In the previous studies of isolated substorms, the magnetotail total pressure was normalized to 22.5 R_E [*Nakai and Kamide*, 2004], and the lobe magnetic field strength was normalized to 25 R_E [*Shukhtina et al.*, 2004]. We also normalize the magnetotail total pressure and lobe magnetic field at the sawtooth onset to

$R = 25\ R_E$ for easy comparison with the previous results. This normalization means that the magnetotail parameters at $R = 25\ R_E$ have these values, but it does not imply that the magnetic reconnection for the sawtooth onset must occur at this location. If a different location is chosen for normalization, there is only a constant factor for all normalized values. The normalized quantities at $R = 25\ R_E$ are written as

$$P_{TN} = P_T(R/25)^{-2.035} \tag{3}$$

and

$$B_{LN} = B_L(R/25)^{-1.0175} \tag{4}$$

[18] In Figures 4a and 4b, the normalized magnetotail total pressure at the sawtooth onset is plotted as a function of the solar wind dynamic pressure and merging electric field. The solar wind pressure is also averaged over 5 min prior to the sawtooth onset. In this study, we use the definition of the merging electric field, $E_m = V_{SW}(B_y^2 + B_z^2)^{1/2}\sin^2(\theta/2)$, given by *Kan and Lee* [1979], where V_{SW} is the solar wind velocity, B_x and B_y are the IMF components, and θ is the IMF clock angle. The merging electric field is averaged over 60 min prior to the sawtooth onset; this 60-min interval presumably corresponds to the accumulation time of the flux in the tail for substorms [*Bargatze et al.*, 1985; *Shukhtina et al.*, 2004, 2005]. The gray line in Figure 4a is the quiet time magnetotail pressure derived by *Nakai and Kamide* [2004]. Plotted in Figures 4c and 4d is the normalized lobe magnetic field at the sawtooth onset, and the gray lines are derived by *Shukhtina et al.* [2004] for isolated substorms. It can be seen that the magnetotail total pressure and lobe magnetic field at the sawtooth onset are systematically higher than the values at the onset of isolated substorms and at quiet times.

[19] The normalized magnetotail total pressure and lobe magnetic field increase with the solar wind pressure and merging electric field, and the empirical formulas are as follows:

$$P_{TN} = 0.25 + 5.21 \times 10^{-2} P_{SW} \tag{5}$$

$$P_{TN} = 0.24 + 4.09 \times 10^{-2} E_m \tag{6}$$

$$B_{LN} = 25.4 + 2.02 P_{SW} \tag{7}$$

$$B_{LN} = 25.0 + 1.56 E_m \tag{8}$$

where P_{TN} is measured with nPa, B_{LN} is measured with nT, the solar wind pressure P_{SW} is measured with nPa, and the merging electric field E_m is measured with mV/m. The small difference in the constant terms are caused by the scatter of the data. The constant terms in P_{TN} and B_{LN} may be explained as the average value of the magnetotail pressure and lobe magnetic field at the equilibrium state, and the increase with the solar wind pressure and merging electric field represents the contribution from the solar wind.

[20] We examine how the normalized magnetotail total pressure and lobe magnetic field vary with the combination of the solar wind pressure and merging electric field. Here we write the combination of the solar wind pressure P_{SW} and merging electric field E_m as

$$Q(P_{SW}, E_m) = P_{SW}^{\alpha} \times E_m^{\delta} \tag{9}$$

We used many different values of α and δ to calculate the minimum variance of the magnetotail parameters and found that the best pair is $\alpha = 0.75$ and $\delta = 1$. The normalized magnetotail total pressure and lobe magnetic field are potted as a function of $Q(P_{SW}, E_m)$ in Figures 4e and 4f.

[21] It is obvious that the scatters of the normalized magnetotail total pressure and lobe magnetic field with respect to $Q(P_{SW}, E_m)$ are smaller than those with respect to the solar wind pressure or merging electric field separately. The regression lines are given by

$$P_{TN} = 0.21 + 2.25 \times 10^{-2} P_{SW}^{0.75} \times E_m \tag{10}$$

$$B_{LN} = 23.9 + 8.76 \times 10^{-1} P_{SW}^{0.75} \times E_m \tag{11}$$

where P_{TN} is in nPa, B_{LN} is in nT, P_{SW} is in nPa, and E_m is in mV/m.

[22] We do not have an explanation as to why the variance of the magnetotail parameters becomes smaller for the function of $Q(P_{SW}, E_m)$ than that for the solar wind pressure or merging electric field. We do not know why the value 0.75 of the power of the solar wind pressure is better than other values (e.g., 0.25, 0.5, 1.0, 1.5, etc). In addition, the solar wind pressure in equations (10) and (11) is the value averaged over 10 min, and the merging electric field is the value averaged over 30 min. We tried different values averaged over 5, 10, 30, and 60 min and found that the 10-min averaged solar wind pressure and 30-min averaged merging electric field give the smallest variance. We also tried the function used by *Shukhtina et al.* [2004] for isolated substorm onsets and found that the variance is very close to those determined by equations (10) and (11). It is unclear whether there are better combinations of the solar wind parameters. These issues need further investigations.

[23] Another important parameter in the magnetosphere is the total magnetic flux stored in the tail lobe. The total flux can be written as $F_T = \pi R_T^2 B_L/2$, where R_T is the radius of the tail lobe and B_L is the lobe magnetic field. We use the empirical formula of the tail radius derived by *Shukhtina et al.* [2004] to calculate the magnetic flux. Figure 5 shows the total magnetic flux as a function of the merging electric field. The gray line is derived by *Shukhtina et al.* [2005] for nonstorm substorms. We also calculated the total magnetic flux with the merging electric field averaged over 30 min and found that the result is almost the same as that with the 60-min averaged merging electric field. This is because the solar wind is often stable for many hours during sawtooth events, and the merging electric field, on average, does not change much from 30 to 60 min. It can be seen in Figure 5 that the total magnetic flux at the sawtooth onset is generally higher than that for isolated substorms (the gray line) and that the difference between sawtooth events and isolated substorms becomes larger as the merging electric field increases.

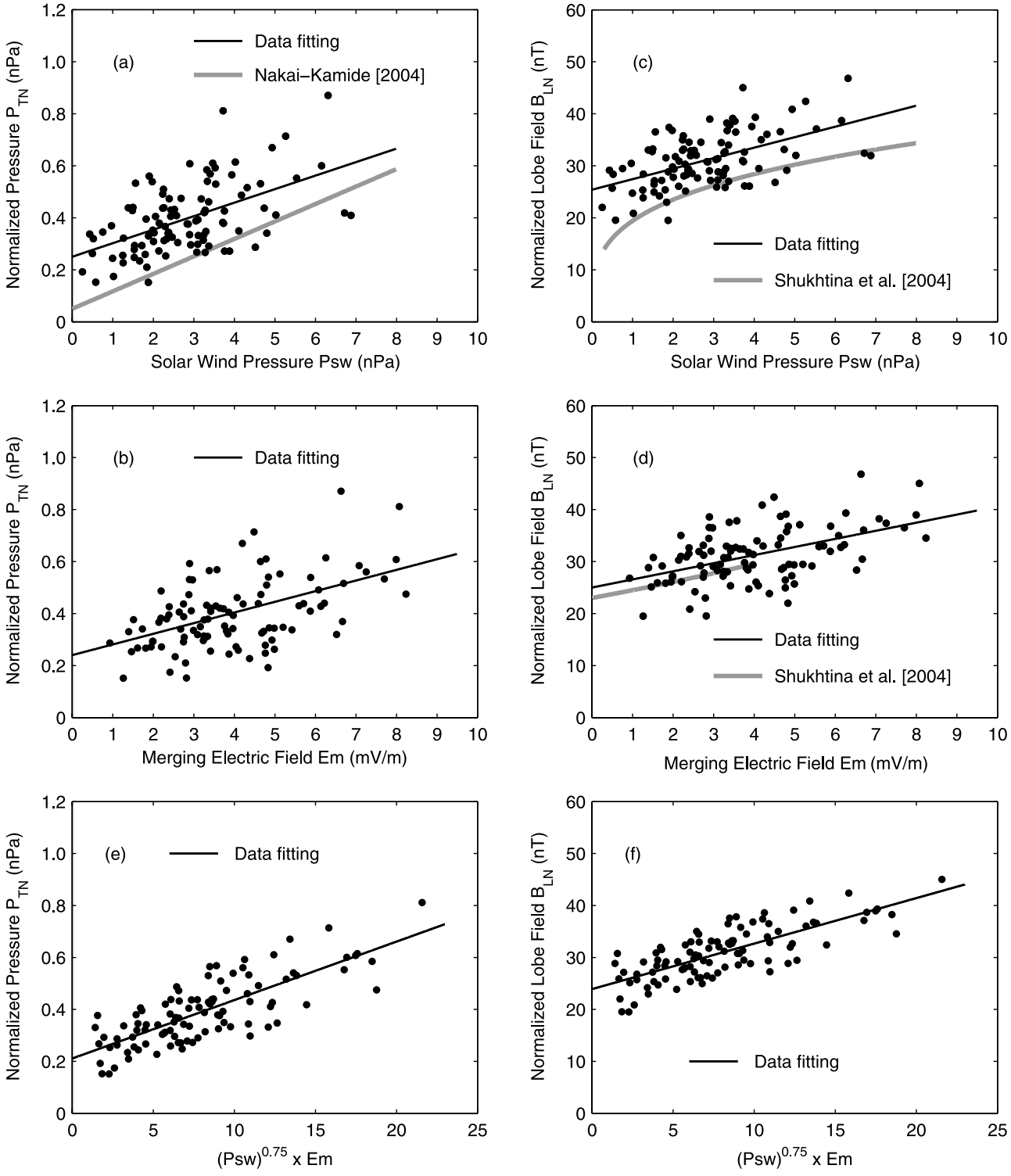

Figure 4. The normalized magnetotail total pressure and lobe magnetic field at the sawtooth onset as a function of the solar wind dynamic pressure, the merging electric field, and the combination of the solar wind dynamic pressure and merging electric field.

2.4. Relationship of Critical Magnetotail Parameters to Storm Strength

[24] The sawtooth events occur mostly during disturbed times. We show here how the magnetotail parameters at the sawtooth onset are related to the strength of magnetic storms. Both the magnetotail total pressure and lobe magnetic field are correlated with the corrected Dst index. We use the formula of *O'Brien and McPherron* [2000] for the corrected Dst index, $Dst_0 = Dst - 7.26P_{SW}^{1/2} + 11$. Similar to the work of *Nakai and Kamide* [2003, 2004], we write the solar wind

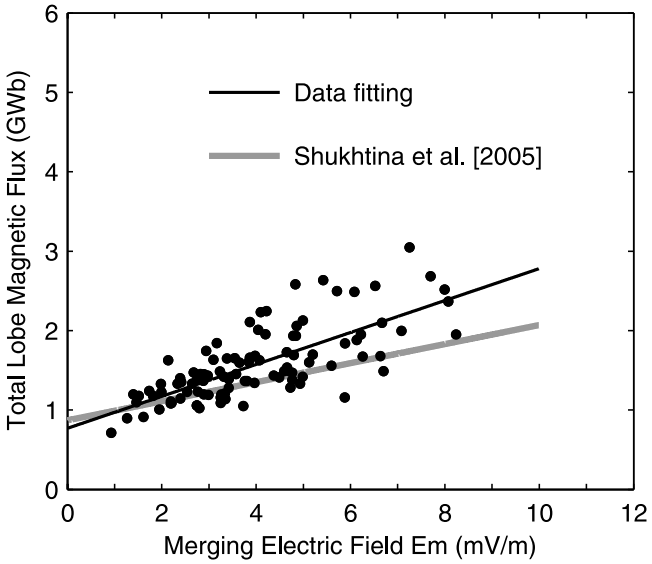

Figure 5. The total magnetic flux in the magnetotail at the sawtooth onset as a function of the merging electric field. The radius of the tail lobe is calculated with the empirical formula of *Shukhtina et al.* [2004].

pressure-corrected, normalized magnetotail total pressure and lobe magnetic field as

$$P_{TNC} = P_{TN} - 5.21 \times 10^{-2}(P_{SW} - \langle P_{SW}\rangle) \tag{12}$$

and

$$B_{LNC} = B_{LN} - 7.26(P_{SW}^{1/2} - \langle P_{SW}\rangle^{1/2}) \tag{13}$$

where $\langle P_{SW}\rangle$ is the mean value of the solar wind pressure and is 2.81 nPa in our data set. The pressure-corrected magnetotail total pressure and lobe magnetic field are plotted in Figure 6, and the regression lines are given by

$$P_{TNC} = 0.28 - 1.77 \times 10^{-3} Dst_0 \tag{14}$$

and

$$B_{LNC} = 26.8 - 7.26 \times 10^{-2} Dst_0 \tag{15}$$

Note that Dst_0 is in general negative during magnetic storms, so the magnetotail total pressure and lobe magnetic field increase with the magnitude of the corrected Dst index.

2.5. Epoch Analysis of the Evolution of Sawtooth Events

[25] We now use the epoch analysis to examine the evolution of the magnetotail total pressure and the lobe magnetic field during sawtooth events. There are 41 teeth (substorms) during which the Geotail satellite was inside the plasma sheet ($\beta > 0.1$) and located between -19 and -31 R_E. The average values of the magnetotail total pressure and lobe magnetic field derived from the 41 substorms are plotted in Figures 7a and 7b. The epoch time is chosen to be the time of the sawtooth onset. Both the magnetotail total pressure and lobe magnetic field show minimum values 78 min before the onset and 77 min after the onset, as marked by the vertical dotted lines. The magnetotail total pressure and lobe magnetic field first increase gradually for 52 min and then rapidly for 26 min. The thick gray lines denote the different stages of the increase, and the vertical dashed line indicates the break of the two stages. If we assume that the interval of 155 min represents the cycle time of the sawtooth events, the gradual increase of the magnetotail pressure and magnetic field over the first 52 min, the rapid increase over the next 26 min, and the continuous decrease over 77 min after the onset may correspond to the recovery phase, growth phase, and expansion phase, respectively. However, it is not clear why the increase of the magnetotail pressure and magnetic field becomes faster during the growth phase than the recovery phase; this issue needs further investigations in the future.

[26] It should be indicated that the three distinct phases in the magnetotail total pressure and lobe magnetic field are caused by the substorm process but not directly by the variation of the solar wind. We plot in Figure 7c the average magnetotail total pressure, merging electric field, and solar

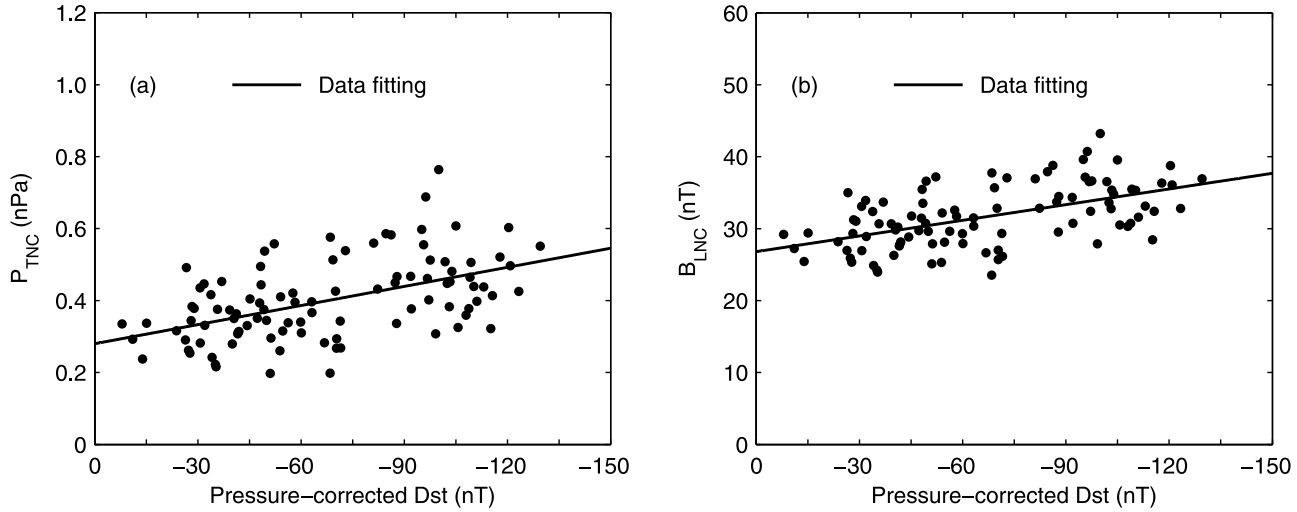

Figure 6. (a) The normalized magnetotail total pressure and (b) the normalized lobe magnetic field at the sawtooth onset as a function of the pressure-corrected Dst index.

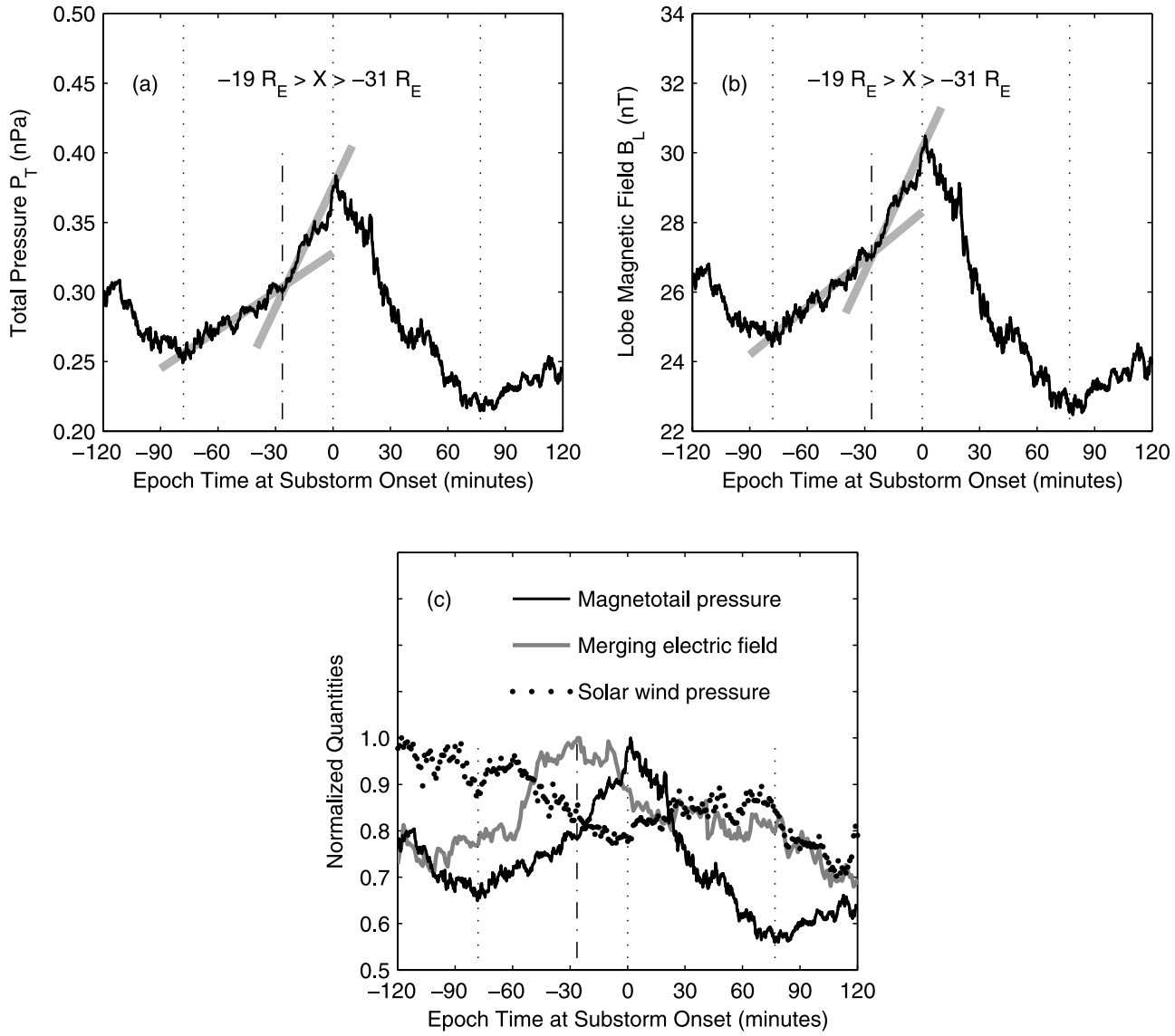

Figure 7. Superposed epoch of (a) the magnetotail total pressure and (b) the lobe magnetic field from 41 teeth (substorms) during sawtooth events. The pressure and magnetic field data were measured by the Geotail satellite between −19 and −31 R_E. (c) Comparison of the variations of the normalized magnetotail total pressure, solar wind pressure, and merging electric field.

wind pressure that have been normalized to their maximum values. The normalized quantities better show the relative variations. The average solar wind pressure decreases during the period of 60 min before the onset time, and the average merging electric field decreases during the period of 26 min before the onset time. In contrast, the magnetotail total pressure, as well as the lobe magnetic field, increases continuously during these periods. Both the merging electric field and solar wind pressure do not have the three-phase characteristics.

2.6. Behaviors of Magnetic Field Strength in Magnetotail

[27] The equivalent lobe magnetic field B_L includes the contribution of the plasma pressure and is different from the magnetic field strength B_T. Here we show how the magnetotail magnetic field strength at the sawtooth onset behaves. In Figure 8a, B_T is plotted as a function of the R distance, and the data regression (the gray line) can be expressed as

$$B_T = 1646R^{-1.349} \tag{16}$$

where B_T is measured with nT. The black line in Figure 8a is the regression line of the lobe magnetic field B_L. It can be seen that B_L is generally larger than B_T, especially for $R >$ 15 R_E. This is because the Geotail satellite is in the plasma sheet in most cases, so the contribution of the plasma pressure to B_L is important. Similar to the practice for B_L, we also normalize B_T to the distance R = 25 R_E and plot the normalized B_T as a function of the solar wind pressure and the merging electric field in Figures 8b and 8c. We then use equation (13) to calculate B_{TNC} and plot B_{TNC} as a function

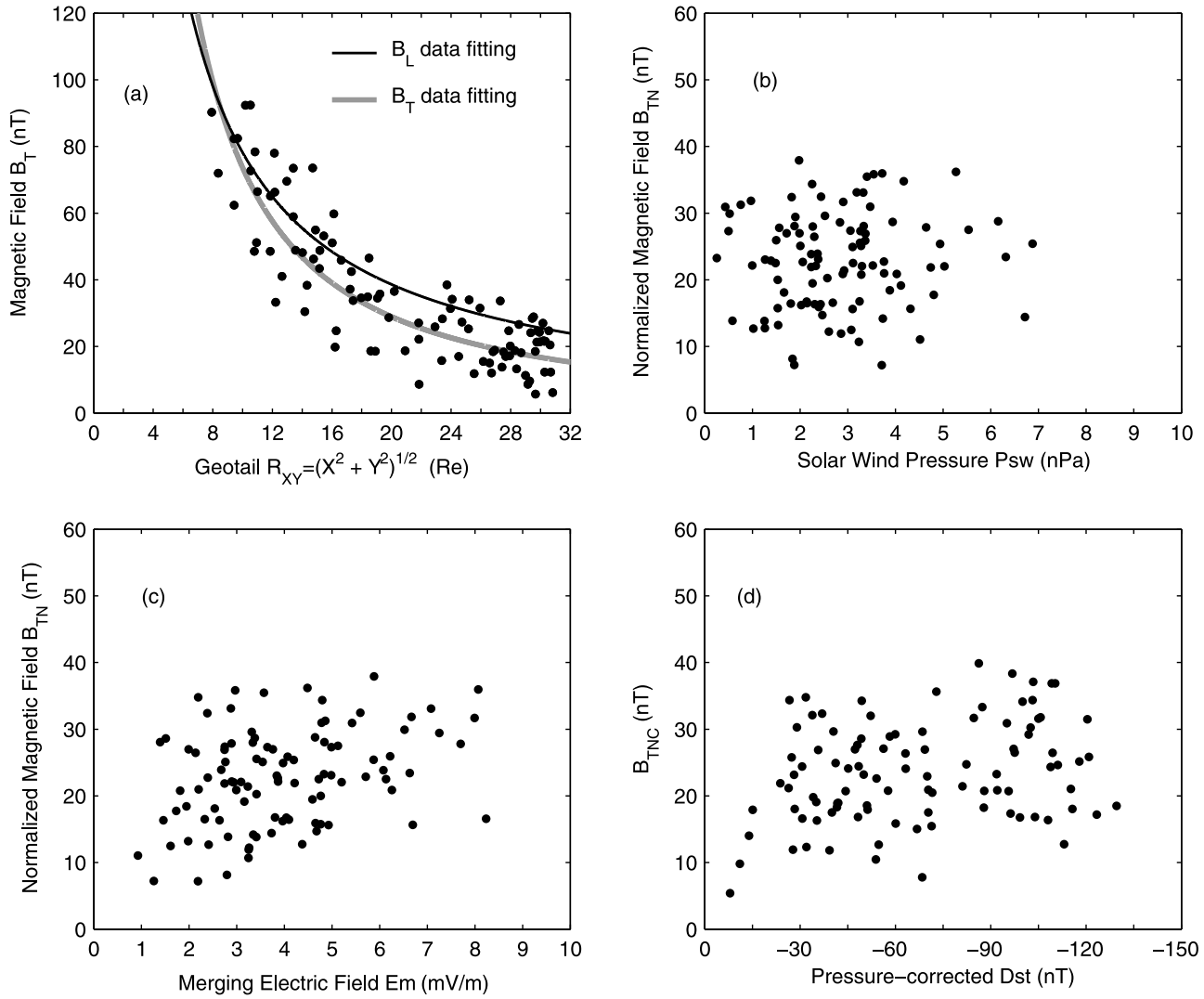

Figure 8. (a) The magnetotail magnetic field at the sawtooth onset as a function of the *R* distance. The normalized magnetic field at the sawtooth onset as a function of (b) the solar wind pressure, (c) the merging electric field, and (d) the pressure-corrected Dst index.

of the corrected Dst index in Figure 8d. Compared with the B_L data in Figures 3b, 4c, 4d, and 6b, the scatters of the B_T data in Figure 8 are much larger.

3. Discussion

[28] We have examined the characteristics of the equivalent lobe magnetic field and total magnetic flux at the sawtooth onset. As can be seen in Figures 4c and 4d, the lobe magnetic field at the sawtooth onset is larger than that at isolated substorms [*Shukhtina et al.*, 2004]. The lobe total magnetic flux for the sawtooth events in Figure 5 is also larger than the flux for isolated substorms [*Shukhtina et al.*, 2005]. This difference may be caused by the IMF (or the merging electric field). The IMF is often strongly southward for many hours in sawtooth events but is generally small in isolated substorms. *DeJong et al.* [2007] calculated the polar cap open magnetic flux during isolated substorms, sawtooth events, and SMC events. They found that the maximum open flux during sawtooth events is larger than that for isolated substorms and SMC events, which is consistent with our results. We plan to compare the tail lobe magnetic flux with the polar cap open magnetic flux in the future.

[29] The temporal variation of the magnetotail parameters in our cases is consistent with the loading-unloading scenario of substorms [*Russell and McPherron*, 1973; *Baker et al.*, 1996]. As shown in Figure 7, the magnetotail total pressure and the lobe magnetic field rapidly increase during the growth phase of the substorms, indicating that the energy from the solar wind is stored in the magnetotail. The magnetotail total pressure and the lobe magnetic field decrease after the onset, indicating that the energy stored in the tail is released during the expansion phase.

[30] Magnetic reconnection in a near-Earth neutral line (NENL) is a widely accepted mechanism responsible for the generation of substorms [*Hones*, 1984; *Baker et al.*, 1996; *Nagai et al.*, 1998]. In this scenario, magnetic flux is transferred from the solar wind to the magnetotail during the growth phase of substorms. As magnetic flux builds up in the tail lobe, the plasma sheet will thin to the scale of an ion

gyroradius, and a global instability, the onset of magnetic reconnection, develops that allows closed field lines to return to the dayside. As described by *Baker et al.* [1996], "the onset of reconnection is attributed to growth phase thinning of the plasma and current sheet, and reduction in the vertical magnetic field through the current sheet. When some portion of the current sheet reaches an appropriate threshold, reconnection begins spontaneously at the center of the sheet." *Birn and Hesse* [1996, 2001] and *Hesse et al.* [2001] simulated the magnetotail current disruption and plasmoid formation. The simulations included a thin current sheet in the near tail region and showed very rapid onset of magnetic reconnection.

[31] The magnetic field in the tail lobe is directly related to the current in the current sheet. If the magnetic reconnection for substorm onset occurs when the current sheet reaches a threshold, it is reasonable to assume that the lobe magnetic field also reaches a threshold. In this study, we have derived the magnetotail total pressure and lobe magnetic field at the sawtooth onset. These magnetotail parameters at the sawtooth onset should correspond to the threshold of the thin current sheet and represent the critical state at which the onset of magnetospheric substorms is about to occur.

[32] However, we cannot exclude the possibility that the substorm onset occurs when other different threshold, rather than the magnetotail total pressure/lobe magnetic field, is reached. More observational investigations and numerical simulations are required to justify whether the sawtooth onset occurs when the magnetospheric parameters reach the critical values derived in this study. In addition, it is not the purpose of this study to determine where the location of the NENL is and whether the NENL is triggered by a current disruption process closer to the Earth [*Lui*, 1996], although our result is consistent with the NENL mechanism.

[33] It is important to note that the critical magnetospheric state at the sawtooth onset depends on the solar wind parameters. The magnetotail parameter (the total pressure, the lobe magnetic field, or the tail lobe magnetic flux) at the sawtooth onset is not a constant but varies with the solar wind pressure/merging electric field. The magnetotail total pressure and lobe magnetic field strength at the sawtooth onsets become higher for stronger solar wind driver.

[34] In fact, this property of the magnetosphere provides a clue for understanding a puzzling phenomenon in the sawtooth events. As reported in previous studies [*Borovsky et al.*, 1993; *Huang*, 2002; *Huang et al.*, 2003a, 2003b, 2004, 2005; *Henderson et al.*, 2006a, 2006b], as well as shown in Figure 1 of this paper, the sawtooth events show a relatively constant period of ~3 hours, although the solar wind driver can be significantly different. The rate of the energy transfer from the solar wind to the magnetotail is higher for stronger southward IMF, so the substorm onset would be expected to occur in a shorter time. In other words, the period of sawtooth events would become shorter for stronger solar wind driver. However, the lobe magnetic field/flux is not constant for all substorms. Instead, the occurrence of sawtooth onsets requires larger lobe magnetic field and total magnetic flux for stronger merging electric field. The amount of the total energy transferred into the magnetotail for the sawtooth onset to occur is greater for higher energy input rate and less for smaller energy input rate. As a result, the time for the magnetotail to reach the critical state is not necessarily shorter for higher energy input rate, and the period of sawtooth events is relatively constant regardless of the strength of the solar wind driver. *Huang et al.* [2003a] suggest that magnetospheric substorms have an intrinsic period of ~3 hours and that the magnetosphere takes ~3 hours after a substorm onset to reach the critical state for the next onset. The findings of this paper support the interpretation of *Huang et al.* [2003a].

4. Conclusions

[35] We have conducted a statistical analysis of the magnetotail parameters measured by the Geotail satellite between −8 and −31 R_E at the onset of storm-time substorms during sawtooth events. The major conclusions are as follows.

[36] (1) The magnetotail total pressure and the equivalent lobe magnetic field show a clearer trend with the radial distance than with the X distance. The magnetotail total pressure at the sawtooth onset is two to three times the pressure at quiet times. The lobe magnetic field at the sawtooth onset is 8−10 nT higher than the quiet time value.

[37] (2) The normalized magnetotail total pressure and lobe magnetic field at the sawtooth onset increase with the solar wind pressure, the merging electric field, and the magnitude of the corrected Dst index. The normalized lobe magnetic field at the sawtooth onset is higher than that at the onset of isolated substorms.

[38] (3) Superposed epoch analysis is used to derive the average characteristics of the temporal evolution of sawtooth events. The magnetotail total pressure and the equivalent lobe magnetic field increase gradually for 52 min and then rapidly for 26 min before the onset and decrease for 77 min after the onset. These three distinct intervals may represent the recovery, growth, and expansion phases of sawtooth events.

[39] (4) The results show that the sawtooth onset occurs when the magnetotail reaches a critical state. However, the critical magnetospheric state is not a constant but depends on the solar wind parameters. The lobe magnetic field and the total magnetic flux must reach a larger value for the onset to occur when the solar wind driver is stronger. Empirical formulas of the relationship between the critical magnetotail parameters at the sawtooth onset and the solar wind are derived. Our findings provide new insight into the storm-time magnetospheric dynamics and important guidance for model simulations.

Appendix A

[40] Here we list the empirical formulas at quiet times and at the onset of isolated substorms derived in previous studies; these formulas were used to compare with the magnetotail parameters at the sawtooth onset in this paper.

[41] The tail lobe magnetic field strength derived by *Fairfield and Jones* [1996, equation (2)] is

$$B_L(\mathrm{nT}) = 1659.22R^{-1.46} + 7.47 \tag{A1}$$

where R is the radial distance and measured with R_E. This formula was derived from the region $-15 > X > -70$ R_E and used to plot the gray line in Figure 3b of our paper.

[42] The magnetotail total pressure derived by *Nakai and Kamide* [2004, equation (1)] is

$$P_T(\mathrm{nPa}) = 25.5R^{-1.59} \tag{A2}$$

This formula was derived from the region $15.0 < R < 30.6\ R_E$ and used to plot the gray line in Figure 3a of our paper.

[43] The tail lobe magnetic field at the onset of isolated substorms derived by *Shukhtina et al.* [2004, equation (5c)] is

$$B_L(\mathrm{nT}) = 23.0(P_d/2.5)^{0.275}(R/25)^{0.739}1.085^{E_m/1.3} \qquad \text{(A3)}$$

where P_d is the solar wind pressure and measured with nPa, and E_m is the merging electric field and measured with mV/m. This formula was derived from the region $-15 > X > -35\ R_E$ and used to plot the gray lines in Figures 4c and 4d of our paper.

[44] The lobe total magnetic flux at the onset of isolated substorms derived by *Shukhtina et al.* [2005, equation (2)] is

$$F_T(\mathrm{GWb}) = 0.87 + 0.12E_m \qquad \text{(A4)}$$

This formula was derived from the region $-15 > X > -32\ R_E$ and used to plot the gray line in Figure 5 of our paper.

[45] **Acknowledgments.** The work at Boston College was supported by National Science Foundation award ATM-0642955. We thank the Geotail team for providing the Geotail magnetic field data (PI: T. Nagai) and plasma data (PI: Y. Saito) through DARTS at Institute of Space and Astronautical Science, JAXA in Japan. We also thank Los Alamos National Laboratory for providing the energetic plasma flux data measured by geosynchronous satellites and the NASA CDAWeb for providing access to the solar wind data.

[46] Wolfgang Baumjohann thanks Robert McPherron and another reviewer for their assistance in evaluating this paper.

References

Baker, D. N., T. I. Pulkkinen, V. Angelopoulos, W. Baumjohann, and R. L. McPherron (1996), Neutral line model of substorms: Past results and present view, *J. Geophys. Res.*, *101*(A6), 12,975–13,010.

Bargatze, L. F., D. N. Baker, R. L. McPherron, and E. W. Hones Jr. (1985), Magnetospheric impulse response for many levels of geomagnetic activity, *J. Geophys. Res.*, *90*(A7), 6387–6394.

Baumjohann, W. G. (1993), The near-Earth plasma sheet: An AMPTE/IRM perspective, *Space Sci. Rev.*, *64*, 141–163.

Baumjohann, W., G. Paschmann, and H. Lühr (1990), Characteristics of high-speed ion flows in the plasma sheet, *J. Geophys. Res.*, *95*(A4), 3801–3809.

Baumjohann, W., Y. Kamide, and R. Nakamura (1996), Substorms, storms, and the near-Earth tail, *J. Geomagn. Geoelectr.*, *48*, 177–185.

Belian, R. D., T. E. Cayton, and G. D. Reeves (1995), Quasi-periodic global substorm generated flux variations observed at geosynchronous orbit, in *Space Plasmas: Coupling Between Small and Medium Scale Processes*, *Geophys. Monogr. Ser.*, vol. 89, edited by M. Ashour-Abdalla, T. Chang, and P. Dusenbery, pp. 143–148, AGU, Washington, D. C.

Birn, J., and M. Hesse (1996), Details of current disruption and diversion in simulations of magnetotail dynamics, *J. Geophys. Res.*, *101*(A7), 15,345–15,358.

Birn, J., and M. Hesse (2001), Geospace environment modeling (GEM) magnetic reconnection challenge: Resistive tearing, anisotropic pressure and Hall effects, *J. Geophys. Res.*, *106*(A3), 3737–3750.

Borovsky, J. E., R. J. Nemzek, and R. D. Belian (1993), The occurrence rate of magnetospheric-substorm onsets: Random and periodic substorms, *J. Geophys. Res.*, *98*(A3), 3807–3813.

Cai, X., C. R. Clauer, and A. J. Ridley (2006), Statistical analysis of ionospheric potential patterns for isolated substorms and sawtooth events, *Ann. Geophys.*, *24*, 1977–1991.

Clauer, C. R., X. Cai, D. Welling, A. DeJong, and M. G. Henderson (2006), Characterizing the 18 April 2002 storm-time sawtooth events using ground magnetic data, *J. Geophys. Res.*, *111*, A04S90, doi:10.1029/2005JA011099.

DeJong, A. D., X. Cai, R. C. Clauer, and J. F. Spann (2007), Aurora and open magnetic flux during isolated substorms, sawteeth, and SMC events, *Ann. Geophys.*, *25*, 1865–1876.

Fairfield, D. H., and J. Jones (1996), Variability of the tail lobe field strength, *J. Geophys. Res.*, *101*(A4), 7785–7791.

Henderson, M. G. (2004), The May 2–3, 1986 CDAW-9C interval: A sawtooth event, *Geophys. Res. Lett.*, *31*, L11804, doi:10.1029/2004GL019941.

Henderson, M. G., G. D. Reeves, R. D. Belian, and J. S. Murphree (1996), Observations of magnetospheric substorms occurring with no apparent solar wind/IMF trigger, *J. Geophys. Res.*, *101*(A5), 10,773–10,791.

Henderson, M. G., G. D. Reeves, R. Skoug, M. T. Thomsen, M. H. Denton, S. B. Mende, T. J. Immel, P. C. Brandt, and H. J. Singer (2006a), Magnetospheric and auroral activity during the 18 April 2002 sawtooth event, *J. Geophys. Res.*, *111*, A01S90, doi:10.1029/2005JA011111.

Henderson, M. G., et al. (2006b), Substorms during the 10–11 August 2000 sawtooth event, *J. Geophys. Res.*, *111*, A06206, doi:10.1029/2005JA011366.

Hesse, M., J. Birn, and M. Kuznetsova (2001), Collisionless magnetic reconnection: Electron processes and transport modeling, *J. Geophys. Res.*, *106*(A3), 3721–3735.

Hones, E. W., Jr. (1984), Plasma sheet behavior during substorms, in *Magnetic Reconnection in Space and Laboratory Plasmas*, *Geophys. Monogr. Ser.*, vol. 30, edited by E. W. Horns Jr., pp. 178–184, AGU, Washington, D. C.

Hsu, T., and R. L. McPherron (2003), Occurrence frequencies of IMF triggered and nontriggered substorms, *J. Geophys. Res.*, *108*(A7), 1307, doi:10.1029/2002JA009442.

Huang, C.-S. (2002), Evidence of periodic (2–3 hour) near-tail magnetic reconnection and plasmoid formation: Geotail observations, *Geophys. Res. Lett.*, *29*(24), 2189, doi:10.1029/2002GL016162.

Huang, C.-S., G. D. Reeves, J. E. Borovsky, R. M. Skoug, Z. Y. Pu, and G. Le (2003a), Periodic magnetospheric substorms and their relationship with solar wind variations, *J. Geophys. Res.*, *108*(A6), 1255, doi:10.1029/2002JA009704.

Huang, C.-S., J. C. Foster, G. D. Reeves, G. Le, H. U. Frey, C. J. Pollock, and J.-M. Jahn (2003b), Periodic magnetospheric substorms: Multiple space-based and ground-based instrumental observations, *J. Geophys. Res.*, *108*(A11), 1411, doi:10.1029/2003JA009992.

Huang, C.-S., G. Le, and G. D. Reeves (2004), Periodic magnetospheric substorms during fluctuating interplanetary magnetic field B_z, *Geophys. Res. Lett.*, *31*, L14801, doi:10.1029/2004GL020180.

Huang, C.-S., G. D. Reeves, G. Le, and K. Yumoto (2005), Are sawtooth oscillations of energetic plasma particle fluxes caused by periodic substorms or driven by solar wind pressure enhancements?, *J. Geophys. Res.*, *110*, A07207, doi:10.1029/2005JA011018.

Kan, J. R., and L. C. Lee (1979), Energy coupling function and solar wind-magnetosphere dynamo, *Geophys. Res. Lett.*, *6*(7), 577–580.

Kokubun, S., T. Yamamoto, M. H. Acuna, K. Hayashi, K. Shiokawa, and H. Kawano (1994), The geotail magnetic field experiment, *J. Geomagn. Geoelectr.*, *46*, 7–21.

Lee, D.-Y., L. R. Lyons, and K. Yumoto (2004), Sawtooth oscillations directly driven by solar wind dynamic pressure enhancements, *J. Geophys. Res.*, *109*, A04202, doi:10.1029/2003JA010246.

Lui, A. T. Y. (1996), Current disruption in the Earth's magnetosphere: Observations and models, *J. Geophys. Res.*, *101*(A6), 13,067–13,088.

Lui, A. T. Y., T. Hori, S. Ohtani, Y. Zhang, X. Y. Zhou, M. G. Henderson, T. Mukai, H. Hayakawa, and S. B. Mende (2004), Magnetotail behavior during storm time "sawtooth injections", *J. Geophys. Res.*, *109*, A10215, doi:10.1029/2004JA010543.

Lyons, L. R., G. T. Blanchard, J. C. Samson, R. P. Lepping, T. Yamamoto, and T. Moretto (1997), Coordinated observations demonstrating external substorm triggering, *J. Geophys. Res.*, *102*(A12), 27,039–27,051.

McPherron, R. L., and T.-S. Hsu (2002), A comparison of substorms occurring during magnetic storms with those occurring during quiet times, *J. Geophys. Res.*, *107*(A9), 1259, doi:10.1029/2001JA002008.

McPherron, R. L., C. T. Russell, and M. P. Aubry (1973), 9. Phenomenological model for substorms, *J. Geophys. Res.*, *78*(16), 3131–3149.

McPherron, R. L., T. Terasawa, and A. Nishida (1986), Solar wind triggering of substorm expansion onset, *J. Geomagn. Geoelectr.*, *38*, 1089–1108.

Mukai, T., S. Machida, Y. Saito, M. Hirahara, T. Terasawa, N. Kaya, T. Obara, M. Ejiri, and A. Nishida (1994), The low energy particle (LEP) experiment onboard the Geotail satellite, *J. Geomagn. Geoelectr.*, *46*, 669–692.

Mukai, T., M. Fujimoto, M. Hoshino, S. Kokubun, S. Machida, K. Maezawa, A. Nishida, Y. Saito, T. Teresawa, and T. Yamamoto (1996), Structure and kinetic properties of plasmoids and their boundary regions, *J. Geomagn. Geolectr.*, *48*, 541–560.

Nagai, T., M. Fujimoto, Y. Saito, S. Machida, T. Terasawa, R. Nakamura, T. Yamamoto, T. Mukai, A. Nishida, and S. Kokubun (1998), Structure and dynamics of magnetic reconnection for substorm onsets with Geotail observations, *J. Geophys. Res.*, *103*(A3), 4419–4440.

Nakai, H., and Y. Kamide (2003), Substorm-associated large-scale magnetic field changes in the magnetotail: A prerequisite for "magnetotail deflation" events, *Ann. Geophys.*, *21*, 869–879.

Nakai, H., and Y. Kamide (2004), A critical condition in magnetotail pressure for leading to a substorm expansion onset: Geotail's observations, *J. Geophys. Res.*, *109*, A01205, doi:10.1029/2003JA010070.

O'Brien, T. P., and R. L. McPherron (2000), An empirical phase space analysis of ring current dynamics: Solar wind control of injection and decay, *J. Geophys. Res.*, *105*(A4), 7707–7719.

Pulkkinen, T. I., N. Y. Ganushkina, E. I. Tanskanen, M. Kubyshkina, G. D. Reeves, M. F. Thomsen, C. T. Russell, H. J. Singer, J. A. Slavin, and J. Gjerloev (2006), Magnetospheric current systems during stormtime sawtooth events, *J. Geophys. Res.*, *111*, A11S17, doi:10.1029/2006JA011627.

Pulkkinen, T. I., N. Partamies, R. L. McPherron, M. Henderson, G. D. Reeves, M. F. Thomsen, and H. J. Singer (2007), Comparative statistical analysis of storm time activations and sawtooth events, *J. Geophys. Res.*, *112*, A01205, doi:10.1029/2006JA012024.

Reeves, G. D., et al. (2003), IMAGE, POLAR, and geosynchronous observations of substorm and ring current ion injection, in *Disturbances in Geospace: The Storm-Substorm Relationship*, *Geophys. Monogr. Ser.*, vol. 142, edited by A. S. Sharma, Y. Kamide, and G. S. Lakhina, pp. 91–101, AGU, Washington, D. C.

Russell, C. T., and R. L. McPherron (1973), The magnetotail and substorms, *Space Sci. Rev.*, *15*, 205–266.

Shukhtina, M. A., N. P. Dmitrieva, and V. S. Sergeev (2004), Quantitative characteristics of different magnetospheric states, *Ann. Geophys.*, *22*, 1019–1032.

Shukhtina, M. A., N. P. Dmitrieva, N. G. Popova, V. A. Sergeev, A. G. Yahnin, and I. V. Despirak (2005), Observational evidence of the loading-unloading substorm scheme, *Geophys. Res. Lett.*, *32*, L17107, doi:10.1029/2005GL023779.

Slavin, J. A., E. J. Smith, B. T. Tsurutani, D. G. Sibeck, H. J. Singer, D. N. Baker, J. T. Gosling, E. W. Hones, and F. L. Scarf (1984), Substorm associated traveling compression regions in the distant tail: Isee-3 geotail observations, *Geophys. Res. Lett.*, *11*(7), 657–660.

Slavin, J. A., R. P. Lepping, J. Gjerloev, D. H. Fairfield, M. Hesse, C. J. Owen, M. B. Moldwin, T. Nagai, A. Ieda, and T. Mukai (2003), Geotail observations of magnetic flux ropes in the plasma sheet, *J. Geophys. Res.*, *108*(A1), 1015, doi:10.1029/2002JA009557.

Taguchi, S., J. A. Slavin, and R. P. Lepping (1998), Traveling compression regions in the midtail: Fifteen years of IMP 8 observations, *J. Geophys. Res.*, *103*(A8), 17,641–17,650.

Weimer, D. R., D. M. Ober, N. C. Maynard, M. R. Collier, D. J. McComas, N. F. Ness, C. W. Smith, and J. Watermann (2003), Predicting interplanetary magnetic field (IMF) propagation delay times using the minimum variance technique, *J. Geophys. Res.*, *108*(A1), 1026, doi:10.1029/2002JA009405.

X. Cai, Bradley Department of Electrical and Computer Engineering, Virginia Tech, 302 Whittemore Hall, Blacksburg, VA 24061, USA. (xcai@vt.edu)

C.-S. Huang, Institute for Scientific Research, Boston College, 402 St Clement's Hall, 140 Commonwealth Avenue, Chestnut Hill, MA 02467, USA. (chaosong.huang.ctr@hanscom.af.mil)